Oscillative Trapping of a Droplet in a Converging Channel Induced by Elastic Instability

Chiyu Xie,[1,2] Pengpeng Qi,[3] Ke Xu,[3,4] Jianping Xu,[3] and Matthew T. Balhoff[2,3,*]
[1]School of Civil and Resource Engineering, University of Science and Technology Beijing, Beijing 100083, China
[2]Center for Subsurface Energy and the Environment, The University of Texas at Austin, Austin, Texas 78712, USA
[3]Hildebrand Department of Petroleum and Geosystems Engineering, The University of Texas at Austin, Austin, Texas 78712, USA
[4]College of Engineering, Peking University, Beijing 100871, China

(Received 19 April 2021; revised 28 November 2021; accepted 13 January 2022; published 3 February 2022)

Permanent trapping of an oscillating, nonwetting droplet is observed in a converging-diverging microchannel when aqueous, viscoelastic fluids are injected. Classical theories based on the balance between capillary and viscous forces suggest that the droplet size should decrease with increasing flow rates of a displacing Newtonian fluid, and the droplet should be completely displaced at high injection rates. However, droplets in viscoelastic fluids cannot be removed by increasing flow rates due to the oscillation. The oscillation amplitude linearly increases with the Deborah number (De), which further inhibits the droplet's passing through the constriction, "permanently." Our microfluidic experiments show that the onset of oscillation is determined by a critical De, which is near 1. We derive a linear relationship for the trapped droplet length with $Ec^{1/3}$, where Ec is the elastocapillary number, by introducing the elastic force into the force balance in addition to the capillary and viscous forces.

DOI: 10.1103/PhysRevLett.128.054502

Viscoelastic fluids are non-Newtonian fluids that act as both viscous fluids and elastic solids simultaneously [1], which play key roles in many natural and industrial fields including biological systems [2,3], food industry [4], and subsurface engineering problems [5,6]. Compared with Newtonian fluids, chaotic flow behaviors can be found in viscoelastic fluids even in the inertia-less limit (Reynolds number, $Re < 1$). These chaotic behaviors include asymmetric vortices in a converging-diverging channel [7–10], secondary flows in the Taylor-Couette flow [11,12], and curved streamlines in driven cavity flow [13]. These phenomena are commonly referred to as "elastic instability" or "elastic turbulence" [14–18].

Efforts on the elastic instabilities have been mainly focused on single-phase flow of viscoelastic fluids through evaluation of curved streamlines. Pakdel and McKinley [13] and McKinley *et al.* [19] found that there exists an onset of elastic instability and characterized it by proposing a group of new dimensionless criteria consisting of the Deborah number (De) and the Weissenberg number (Wi) for various simple flow geometries. McKinley's criteria have been also applied to explain the elastic instabilities observed in microfluidic porous networks [20,21]. Walkama *et al.* [21] further demonstrated that introducing a small disorder into the porous geometry can suppress the elastic instabilities because the induced preferential flow paths promote shear over extensional deformation.

There have also been a few studies on the free surface elastic instabilities, which do not involve curved streamlines, such as the jet breakup during filament stretching [22–24] and the liquid sheet instability [25,26]. However, only limited studies addressing the instability behaviors in disperse multiphase flows of viscoelastic fluids are available in the literature. Clarke *et al.* [27,28] discovered fluctuations of residual oil droplets in a glass, porous micromodel when displaced by viscoelastic solutions. Our recent work [29] provided numerical evidence of droplet oscillation by viscoelastic fluids and demonstrated that viscoelastic oscillation can help mobilize droplets from their originally trapped positions.

The purpose of this Letter is to show a new way for the manipulation of droplets by demonstrating experimentally and quantifying the newfound droplet trapping and oscillation in viscoelastic fluids. The experiments are performed in a converging-diverging microfluidic channel, which is a simple but important geometry to investigate many fundamental flow processes, such as droplet generation and snap-off [30–32]. Specifically, we show that (i) the linear relationship between the critical trapped droplet length and $Ca^{-1/3}$ (Ca is the capillary number) for Newtonian fluids proposed by Xu *et al.* [33] only holds for viscoelastic fluids below a critical De; (ii) the elastocapillary number ($Ec = De/Ca$), originally named by McKinley [34] for inertialess flows of free surface viscoelastic fluids, can be applied to analyze the viscoelastic oscillation; and (iii) the relationship between De and the oscillation amplitude can be quantified.

The viscoelastic oscillation is a strongly coupled phenomenon involving a balance of the elastic (F_{els}) and viscous forces (F_{vis}) in addition to the capillary force (F_{cap}). All the

experiments presented here are in the inertialess limit [14] (the maximum Reynolds number for all cases in this study is $\mathrm{Re} = 0.2 < 1$), therefore, the main dimensionless groups governing this process are defined as

$$\mathrm{De} = \frac{\tau U}{L} \propto \frac{F_{\mathrm{els}}}{F_{\mathrm{vis}}}, \tag{1a}$$

$$\mathrm{Ca} = \frac{\eta U}{\gamma} \propto \frac{F_{\mathrm{vis}}}{F_{\mathrm{cap}}}, \tag{1b}$$

$$\mathrm{Ec} = \frac{\mathrm{De}}{\mathrm{Ca}} = \frac{\tau\gamma}{\eta L}, \tag{1c}$$

where τ is the viscoelastic relaxation time, η is the dynamic viscosity of the displacing fluid, γ is the interfacial tension, U is the characteristic velocity, and L is the characteristic length. The Deborah number (De) represents the ratio of elastic to viscous forces, the capillary number (Ca) represents the ratio of viscous to capillary forces, and the elastocapillary number (Ec) accounts for the combined importance of elastic and capillary forces, compared to the viscous force.

The microfluidic experimental platform and geometry of the single converging-diverging channel is shown in Fig. S1 [35], which contains two main channels (50 mm in length, 300 μm in width, and 45 μm in depth) connected by a throat (300 μm in length, 60 μm in width, and 15 μm in depth). We compare the displacements of a Newtonian fluid (F_{N0}: tetradecane) through this microchannel by both viscoelastic and inelastic fluids (Table S1 [35]). The viscoelastic fluids (F_{VE1} to F_{VE4}) include two hydrolyzed polyacrylamide (HPAM) polymer solutions and two polyethylene oxide in polyethylene glycol solutions of varying molecular weight and concentration, and therefore different relaxation times. The inelastic fluids include both Newtonian fluids (F_{N1}:50% glycerol solution, and F_{N2}:brine) and shear-thinning fluids (F_{S1}:0.075% scleroglucan solution, and F_{S2}:0.1%, 8M Mw HPAM solution). See also Supplemental Material [35] for more details about the microfluidic geometry and fluid properties.

The dry microchannel is initially saturated with brine to ensure a completely water-wet condition. Then the Newtonian fluid F_{N0} (droplet) is slowly (1 μL/h) injected to fully displace the brine. The displacing, wetting fluid is then injected at a low flow rate (0.2 μl/h). Since the microchannel is completely water wet, a droplet is generated upstream of the throat and trapped due to capillary forces. The injection rate (and thus the capillary number) is then incrementally increased until the droplet is either pushed through or the droplet size no longer decreases (usually results in oscillation upstream of the throat). Snapshots of the droplet at each steady state are recorded for image analysis to obtain the effective droplet length L (the area of the droplet divided by the width of the main channel) as the characteristic length. The mean velocity at the inlet (U = flow rate divided by cross-sectional area of the main channel) is taken as the characteristic velocity.

Typical snapshots for the trapped droplet (F_{N0}) during displacements by different fluids at various flow rates are shown in Fig. 1. For all inelastic cases, the droplet length decreases with increasing flow rate, and the droplet completely passes through the throat at high flow rates ($\mathrm{Ca} > 4 \times 10^{-5}$). While for all viscoelastic cases, the droplet no longer decreases in length at high flow rates

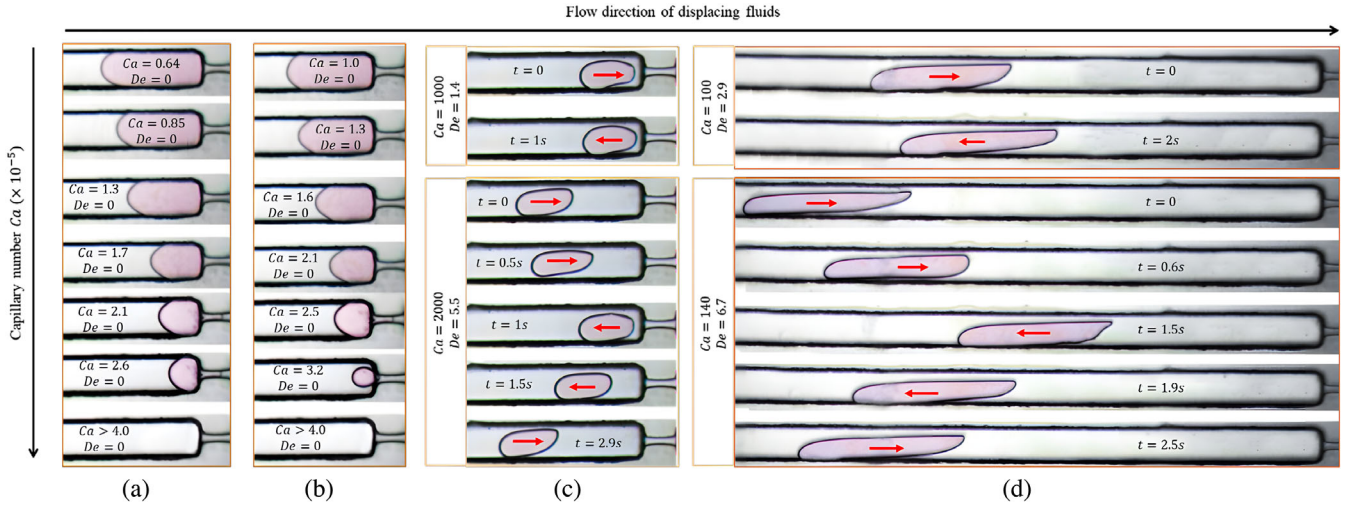

FIG. 1. Viscoelastic fluids induce droplet oscillation. Typical snapshots for the trapped droplets during displacements by (a) Newtonian fluid F_{N1} at flow rates from 1.5 μL/h to 6 μL/h, (b) shear-thinning fluid F_{S1} at flow rates from 0.1 μL/h to 0.35 μL/h, (c) viscoelastic fluid F_{VE4} with a lower relaxation time ($\tau = 0.41$ s) at flow rates of 50 μL/h and 200 μL/h, and (d) viscoelastic fluid F_{VE1} with a higher relaxation time ($\tau = 2$ s) at flow rates of 70 μL/h and 160 μL/h. The red arrows in (c) and (d) indicate the moving direction of the oscillating droplets.

(De > 1), but instead oscillates in the main channel upstream of the throat and is trapped permanently. The droplet is pushed toward the throat, then changes direction toward the inlet until it stops and changes direction again toward the throat. No oscillation occurs for displacements by inelastic fluids (including shear-thinning fluids F_{S1} and F_{S2}). Comparing the displacements using fluids F_{S1} and F_{VE1} that the oscillation only occurs in the latter case, we can exclude the shear-thinning behavior of non-Newtonian fluids as a factor for oscillation since both fluids have similar shear-thinning rheology (Fig. S2 [35]) but only fluid F_{VE1} is viscoelastic. We also reverse the process by using the Newtonian fluid F_{N0} as the bulk fluid to displace a viscoelastic droplet (F_{VE3}), showing completely displacement and no oscillation of the droplet (Fig. S5 [35]). Therefore, we further confirm that it is the viscoelasticity of the displacing fluids that results in the droplet oscillation. Streamline analysis by the particle image velocimetry (PIV) measurement (Fig. S6 [35]) and our numerical simulation [29] also proved that the oscillation is caused by elastic instability and turbulence. See also Fig. S4 [35] for displacements by all other fluids and Supplemental Material movies [35] for the dynamic viscoelastic oscillation processes.

For inelastic fluids, Xu *et al.* [33] showed the displacement is only determined by the force balance of viscous and capillary forces (derived by Wong *et al.* [44,45]) as follows:

$$F_{\mathrm{vis}} \propto \eta U L, \tag{2a}$$

$$F_{\mathrm{cap}} \propto \eta U \mathrm{Ca}^{-1/3}. \tag{2b}$$

Therefore, a linear relationship between $\tilde{L}$ and $\mathrm{Ca}^{-1/3}$ was derived, where $\tilde{L}$ is the dimensionless form of the effective droplet length L as $\tilde{L} = L/w$ ($w = 300$ μm is the main channel width). As shown in Fig. 2, for all inelastic displacements, the size of the droplet decreases as Ca increases, and data agree with this relationship. For viscoelastic displacements, we find the data also overlap with the inelastic data at low flow rates (De < 1), but the results deviate from the linear trend near the onset of viscoelastic oscillation.

Figure 2 also indicates that the final length (L_∞) of the oscillating droplets at high velocities varies for different viscoelastic experiments. To determine the impact of fluid properties and flow conditions on the final droplet length, the critical condition for the onset of oscillation [Fig. 3(e)] must be determined, as L_∞ no longer changes once the oscillation starts.

We track the evolution of the distance [Fig. 3(a)] between the droplet center to the throat entrance for all the viscoelastic displacements, and Fig. 3(b) shows the displacement by viscoelastic fluid F_{VE4} at the flow rate of 250 μL/h (De = 6.9). By applying a high pass fast Fourier transform (FFT) filter, the data of Fig. 3(b) are further

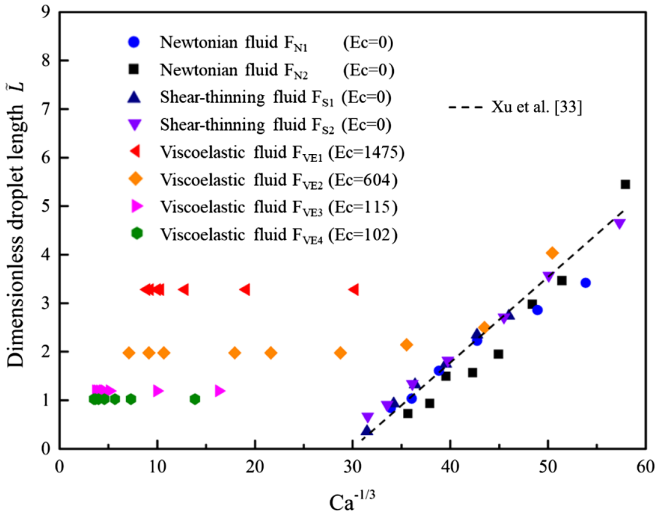

FIG. 2. The dimensionless length of the trapped droplet $\tilde{L}$ with respect to $\mathrm{Ca}^{-1/3}$. The dash line is a linear fit to the inelastic data according to Xu *et al.* [33].

analyzed and converted to Fig. 3(c), which indicates that each oscillation follows a wave with a constant amplitude A. These amplitudes are plotted against De in Fig. 3(d), showing an increasing trend with De, nearly linearly, with some scatter:

$$\tilde{A} = m(\mathrm{De} - \mathrm{De}_{\mathrm{crit}}), \tag{3}$$

where $\tilde{A} = A/L_\infty$ is the dimensionless amplitude and the slope m is dependent on the converging-diverging geometry and is 0.177 in our experiments. See also Supplemental Material [35] for more details on the derivation of Eq. (3) based on the theory of simple harmonic motion. Figure 3(d) further indicates the critical condition for the onset of viscoelastic oscillation, which is determined by De as $\mathrm{De}_{\mathrm{crit}}$ is around 1 in our experiments.

At the onset of oscillation (critical condition), all three forces are balanced as

$$F_{\mathrm{vis}} = F_{\mathrm{cap}} + F_{\mathrm{els}}. \tag{4}$$

According to Eqs. 1(a) and (2), we have

$$F_{\mathrm{vis}} = \varphi \eta U_{\mathrm{crit}} L_\infty, \tag{5a}$$

$$F_{\mathrm{cap}} = \psi \eta U_{\mathrm{crit}} \mathrm{Ca}_{\mathrm{crit}}^{-1/3}, \tag{5b}$$

$$F_{\mathrm{els}} = \chi \mathrm{De}_{\mathrm{crit}} F_{\mathrm{vis}} = \chi \eta U_{\mathrm{crit}} \mathrm{De}_{\mathrm{crit}} L_\infty, \tag{5c}$$

where φ, ψ, and χ are geometric coefficients. Then by substituting Eq. (5) into Eq. (4), we obtain

$$\tilde{L}_\infty \propto \mathrm{Ca}_{\mathrm{crit}}^{-1/3}/(1 - \alpha \mathrm{De}_{\mathrm{crit}}), \tag{6}$$

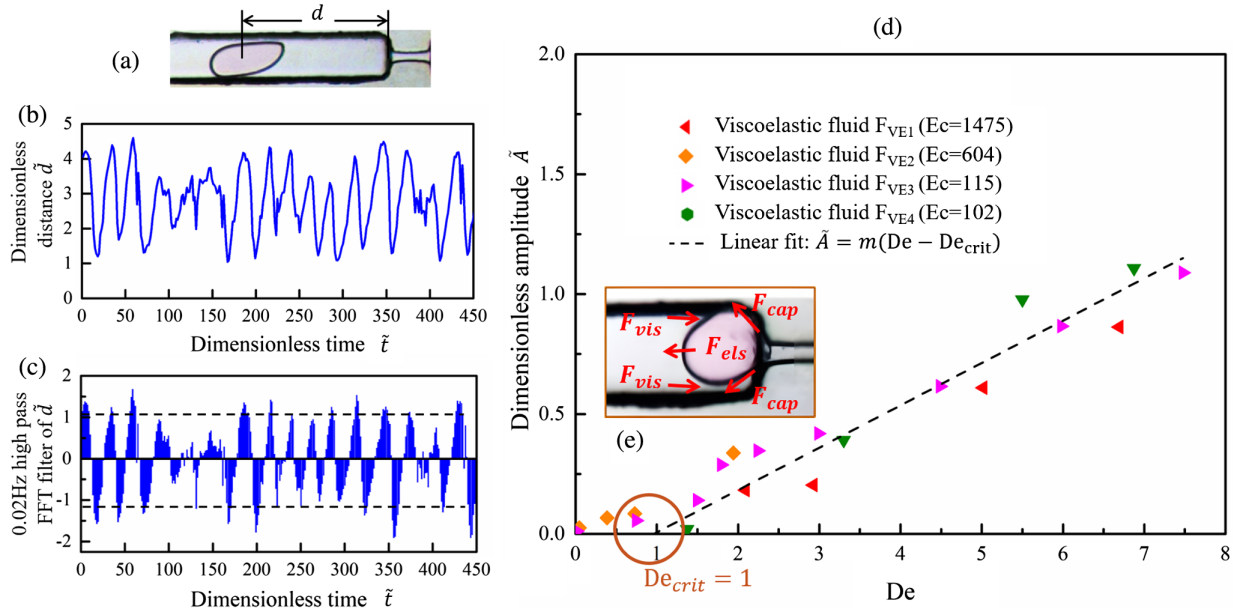

FIG. 3. The effect of Deborah number De on the oscillation amplitude. (a) Definition of the distance d between the droplet mass center to the throat entrance. (b) The evolution of the dimensionless distance $\tilde{d} = d/L_\infty$ for viscoelastic fluid F_{VE4} at the flow rate of 250 μL/h (De = 6.9) as an example. The time t is nondimensionalized by L_∞/U as $\tilde{t} = tU/L_\infty$. (c) A 0.02 Hz high pass fast Fourier transform (FFT) filter on the data of Fig. 3(b) to obtain the oscillation amplitude. The dashed lines denote the average dimensionless amplitude $\tilde{A}$. (d) The dimensionless oscillation amplitude $\tilde{A}$ of the droplet with respect to De. The dashed line is a linear fit to all the data. (e) The forces excerted on the droplet at the onset of oscillation (the droplet is about to detach from the throat entrance) for the displacement by viscoelastic fluid as an illustration.

where $\alpha = \chi/\varphi$, $\tilde{L}_\infty$ is the final dimensionless length of the oscillating droplet, nondimensionalized by the main width ($w = 300$ μm). $\tilde{L}_\infty = L_\infty/w$. Equation (6) can be rewritten by introducing the elastocapillary number [Eq. 1(c)]:

$$\tilde{L}_\infty \propto \frac{\mathrm{De}_{\mathrm{crit}}^{-1/3}}{1 - \alpha \mathrm{De}_{\mathrm{crit}}} \mathrm{Ec}^{1/3}. \tag{7}$$

Since $\mathrm{De}_{\mathrm{crit}}$ ($\sim$1) and α (a geometric coefficient) are both constants, we obtain a linear relationship between $\tilde{L}_\infty$ and $\mathrm{Ec}^{1/3}$. Our data for the viscoelastic fluids also demonstrate this relationship as shown in Fig. 4 [where the slope ε should be proportional to the coefficient in Eq. (7), and is 0.26 in our experiments], which indicates that the final oscillation length of the droplet is only determined by the fluid properties and is independent of flow rate.

In this Letter, we experimentally show oscillation and permanent trapping of a nonwetting droplet in a converging-diverging microfluidic channel induced by elastic instability. We demonstrate this phenomenon occurs only if the displacing fluid is viscoelastic. There exists a critical De for the onset of viscoelastic oscillation, which is found to be around 1 in our experiments. The oscillation amplitude is found to increase with De linearly beyond the critical De. Because of viscoelastic oscillation and trapping, the linear relationship between the critical trapped droplet length and $\mathrm{Ca}^{-1/3}$ originally derived for Newtonian displacements is no longer valid for viscoelastic displacements. This is because the elastic force must be considered in addition to the capillary and viscous forces. Analysis of the force balance at the onset of oscillation (critical De), we discover a linear relationship between the final trapped droplet length and $\mathrm{Ec}^{1/3}$, which emphasizes the importance of the elastocapillary number (Ec) for inertialess multiphase

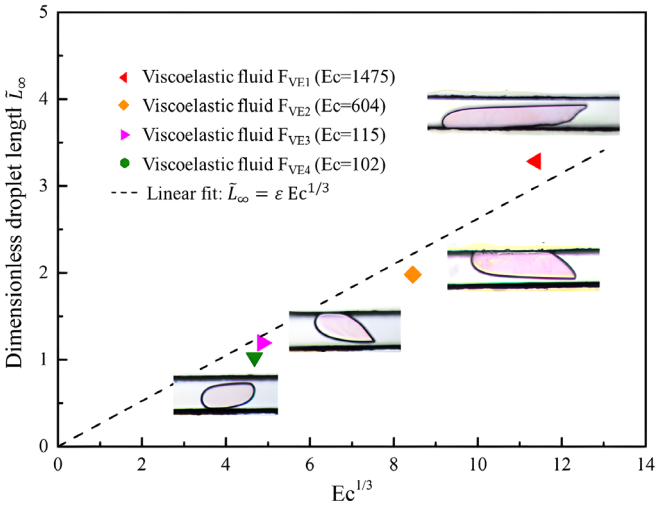

FIG. 4. The dimensionless length of the oscillating droplet $\tilde{L}_\infty$ with respect to $\mathrm{Ec}^{1/3}$. The insets are snapshots of the droplets during oscillation.

flows of viscoelastic fluids. This discovery presents a novel consequence of viscoelastic instability for a viscoelastic fluid in the presence of another fluid, and provides new possibilities for trapping and manipulation of droplet in microstructures.

We thank K. Mohanty, H. Song, and J. Jin for assistance with the fluid preparation and rheology tests. This work was supported by the Chemical EOR Industrial Affiliates Project in the Center for Subsurface Energy and the Environment at UT-Austin.

*Corresponding author.
balhoff@mail.utexas.edu

[1] M. M. Denn, Annu. Rev. Fluid Mech. **22**, 13 (1990).
[2] N. Bessonov, A. Sequeira, S. Simakov, Yu. Vassilevskii, V. Volpert, and V. Volpert, Math. Model. Nat. Phenom. **11**, 1 (2016).
[3] M. Brust, C. Schaefer, R. Doerr, L. Pan, M. Garcia, P. E. Arratia, and C. Wagner, Phys. Rev. Lett. **110**, 078305 (2013).
[4] M. A. Rao, in *Rheology of Fluid and Semisolid Foods: Principles and Applications*, edited by G. V. Barbosa-Canovas (Springer, Boston, 2007), p. 153.
[5] K. S. Sorbie, *Polymer-Improved Oil Recovery* (Springer Science & Business Media, New York, 2013).
[6] K. C. Taylor and H. A. Nasr-El-Din, J. Pet. Sci. Eng. **19**, 265 (1998).
[7] L. E. Rodd *et al.*, J. Non-Newton Fluid **143**, 170 (2007).
[8] D. V. Boger, Annu. Rev. Fluid Mech. **19**, 157 (1987).
[9] R. Keunings and M. J. Crochet, J. Non-Newton Fluid **14**, 279 (1984).
[10] A. M. Afonso, P. J. Oliveira, F. T. Pinho, and M. A. Alves, J. Fluid Mech. **677**, 272 (2011).
[11] S. J. Muller, R. G. Larson, and E. S. Shaqfeh, Rheol. Acta **28**, 499 (1989).
[12] R. G. Larson, E. S. G. Shaqfeh, and S. J. Muller, J. Fluid Mech. **218**, 573 (1990).
[13] P. Pakdel and G. H. McKinley, Phys. Rev. Lett. **77**, 2459 (1996).
[14] A. Groisman and V. Steinberg, Nature (London) **405**, 53 (2000).
[15] A. Groisman and V. Steinberg, New J. Phys. **6**, 29 (2004).
[16] J. Page, Y. Dubief, and R. R. Kerswell, Phys. Rev. Lett. **125**, 154501 (2020).
[17] S. S. Datta *et al.*, arXiv:2108.09841.
[18] C. A. Browne and S. S. Datta, Sci. Adv. **7**, j2619 (2021).
[19] G. H. McKinley, P. Pakdel, and A. Öztekin, J. Non-Newton Fluid **67**, 19 (1996).
[20] A. M. Howe, A. Clarke, and D. Giernalczyk, Soft Matter **11**, 6419 (2015).
[21] D. M. Walkama, N. Waisbord, and J. S. Guasto, Phys. Rev. Lett. **124**, 164501 (2020).
[22] H. K. Rasmussen and O. Hassager, J. Rheol. **45**, 527 (2001).
[23] P. P. Bhat, S. Appathurai, M. T. Harris, M. Pasquali, G. H. McKinley, and O. A. Basaran, Nat. Phys. **6**, 625 (2010).
[24] H. Kibbelaar, A. Deblais, F. Burla, G. H. Koenderink, K. P. Velikov, and D. Bonn, Phys. Rev. Fluids **5**, 092001 (2020).
[25] R. Duan, Z.-y. Chen, C. Wang, and L.-j. Yang, J. Fluids Eng. **135**, 121204 (2013).
[26] T. Hu, Q.-f. Fu, Y. Xing, L.-j. Yang, and L. Xie, Phys. Rev. Fluids **6**, 083902 (2021).
[27] A. Clarke, A. M. Howe, J. Mitchell, J. Staniland, and L. A. Hawkes, SPE J. **21**, 675 (2016).
[28] J. Mitchell, K. Lyons, A. M. Howe, and A. Clarke, Soft Matter **12**, 460 (2016).
[29] C. Xie, K. Xu, K. Mohanty, M. Wang, and M. T. Balhoff, Phys. Rev. Fluids **5**, 063301 (2020).
[30] J. G. Roof, Soc. Pet. Eng. J. **10**, 85 (1970).
[31] C. Zhou, P. Yue, and J. J. Feng, Phys. Fluids **18**, 092105 (2006).
[32] P. Sajeesh and A. K. Sen, Microfluid Nanofluid **17**, 1 (2014).
[33] K. Xu, P. Zhu, C. Huh, and M. T. Balhoff, Langmuir **31**, 13673 (2015).
[34] G. H. McKinley, SOR Rheol. Bull. **74**, 6 (2005), http://www0.rheology.org/sor/publications/rheology_b/RB2005Jul.pdf.
[35] See Supplemental Material at http://link.aps.org/supplemental/10.1103/PhysRevLett.128.054502, which includes Refs. [36–43], for details of the experimental details, and supplemental figures and movies.
[36] H. Song, G. A. Pope, and K. K. Mohanty (Society of Petroleum Engineers, 2020), 10.2118/199921-MS.
[37] E. Volpert, J. Selb, and F. Candau, Polymer **39**, 1025 (1998).
[38] V. Castelletto, I. W. Hamley, W. Xue, C. Sommer, J. S. Pedersen, and Peter D. Olmsted, Macromolecules **37**, 1492 (2004).
[39] P. Qi, D. H. Ehrenfried, H. Koh, and M. T. Balhoff, SPE J. **22**, 447 (2017).
[40] M. Z. Erincik *et al.*, SPE J. **05**, 1944 (2018).
[41] R. Mezzenga, C. Meyer, C. Servais, A. I. Romoscanu, L. Sagalowicz, and R. C. Hayward, Langmuir **21**, 3322 (2005).
[42] T. Shaw, M. Winston, C. J. Rupp, I. Klapper, and P. Stoodley, Phys. Rev. Lett. **93**, 098102 (2004).
[43] S. Liu, S. Shankar, M. C. Marchetti, and Y. Wu, Nature (London) **590**, 80 (2021).
[44] H. Wong, C. J. Radke, and S. Morris, J. Fluid Mech. **292**, 71 (1995).
[45] H. Wong, C. J. Radke, and S. Morris, J. Fluid Mech. **292**, 95 (1995).